

Article

# Preparation and Characterization of Rh/MgSNTs Catalyst for Hydroformylation of Vinyl Acetate: The Rh<sup>0</sup> was Obtained by Calcination

Penghe Su <sup>1</sup>, Ya Chen <sup>1</sup>, Xiaotong Liu <sup>1</sup>, Hongyuan Chuai <sup>1</sup>, Hongchi Liu <sup>1</sup>, Baolin Zhu <sup>1,2</sup>, Shoumin Zhang <sup>1,2</sup> and Weiping Huang <sup>1,2,3,\*</sup>

<sup>1</sup> College of Chemistry, Nankai University, Tianjin 300071, China; sph\_edu@163.com (P.S.); xiaoyayaking@163.com (Y.C.); jenalia@163.com (X.L.); chuaihongyuan0108@163.com (H.C.); h335liu@edu.uwaterloo.ca (H.L.); zhubaolin@nankai.edu.cn (B.Z.); zhangsm@nankai.edu.cn (S.Z.)

<sup>2</sup> The Key Laboratory of Advanced Energy Materials Chemistry (Ministry of Education), Nankai University, Tianjin 300071, China

<sup>3</sup> Collaborative Innovation Center of Chemical Science and Engineering, Tianjin 300071, China

\* Correspondence: hwp914@nankai.edu.cn; Tel.: +86-138-2009-6974

Received: 01 February 2019; Accepted: 18 February 2019; Published: 26 February 2019

**Abstract:** A simple and practical Rh-catalyzed hydroformylation of vinyl acetate has been synthesized via impregnation-calcination method using silicate nanotubes (MgSNTs) as the supporter. The Rh<sup>0</sup> (zero valent state of rhodium) was obtained by calcination. The influence of calcination temperature on catalytic performance of the catalysts was investigated in detail. The catalysts were characterized in detail by X-ray diffraction (XRD), transmission electron microscopy (TEM), X-ray photoelectron spectrometer (XPS), atomic emission spectrometer (ICP), and Brunauer–Emmett–Teller (BET) surface-area analyzers. The Rh/MgSNTs(a<sub>2</sub>) catalyst shows excellent catalytic activity, selectivity and superior cyclicity. The catalyst could be easily recovered by phase separation and was used up to four times.

**Keywords:** silicate nanotubes; Rh; hydroformylation; vinyl acetate

## 1. Introduction

Hydroformylation allows atom-efficient and direct formation of aldehydes from olefins and synthesis gas, and has become a powerful synthetic route for the preparation of some key organic intermediates [1]. Recently, hydroformylation of functionalized olefins has received considerable attention [2], especially in the aspect of some special olefins, cycloolefins [3], vinyl acetate [4–6], dicyclopentadiene (DCPD) [7,8] and 1,3-Butadiene [9]. Because their aldehyde products, especially linear products, can be used to prepare of a variety of biologically active compounds and fine chemicals, such as chiral alcohols, acids, amines, diols, and amino alcohols [10,11]. At present, hydroformylation is the largest application of homogeneous catalysis on an industrial scale with a capacity of more than 10 million tons per year, and is almost exclusively targeted to the production of the linear aldehydes [12]. However, for hydroformylation of vinyl acetate, the selectivity of linear aldehyde (3-acetoxy propanal) is mostly less than 5% among the existing reports [4–6].

Owing to lower reaction temperature and pressure, nano-Rh-based catalysts have been widely used in hydroformylation reactions [13,14]. In particular, supported Rh catalysts have emerged as very active catalysts for hydroformylation of olefins [15,16]. It is generally known that several factors can limit the development of gas phase ethanol oxidation with supported Rh catalysts. In particular, the reaction generally requires a high temperature, which tends to cause sintering of the Rh nanoparticles and hence low selectivity. For some oxide-supported Rh catalysts TNTs [17,18], ZrO<sub>2</sub> [19], ZnO [20], MgO [21], mesoporous MCM-41 and SBA-15 [22], molecular sieve [23], porous

organic polymers [24], Rh nanoparticles are prone to sintering caused by Ostwald ripening, coalescence, or particle migration due to the weak metal-support interactions. Therefore, it is welcome to improve the thermal stability of Rh nanoparticles on supports. We have recently reported that Rh/TiO<sub>2</sub> showed low temperature vinyl acetate conversion (~100%) at ~100 °C, but relatively low acetaldehyde selectivity (~0%) [25]. Therefore, identifying a robust catalyst with a unique combination of excellent catalytic activity, selectivity, and good resistance to sintering is highly desirable from both an academic and industrial standpoint

Magnesium silicate nanotubes (MgSNTs) have high specific surface area (SSA) and one-dimensional tubular structure, strong adsorption capacity, larger pore size and outstanding thermal stability. Therefore, MgSNTs are suitable as carriers of catalysts. They can effectively disperse and immobilize metal active components, improve catalytic activity and stability, and overcome the disadvantages of hard separation catalysts and production in homogeneous catalytic systems. Chen [26] repeated MgSNTs supported Au catalyst to catalyze selective oxidation of ethanol to acetaldehyde, and obtained good results. Not long ago, we reported nanotubular MgSNTs-supported amorphous Co-B catalysts and their catalytic performances for Hydroformylation of cyclohexene [27], which proved that MgSNTs are indeed good supporters for hydroformylation.

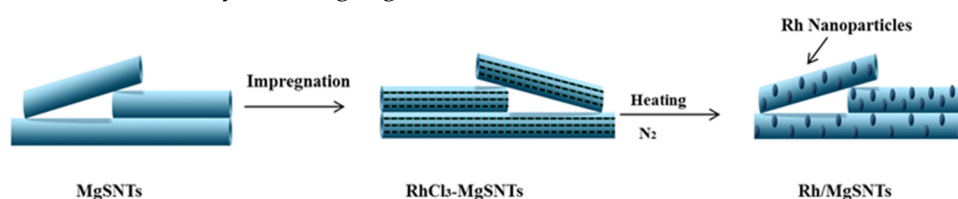
In this study, we report the design and synthesis of Rh-catalysts supported on MgSNTs via the calcination method under N<sub>2</sub>, which has been reported rarely by literatures. The Rh/MgSNTs exhibited a considerable impact on the hydroformylation of vinyl acetate and provided excellent regioselectivity (9%) to linear aldehyde (3-acetoxy propanal), which is much higher than recent reports [28,29] and this should be due to the confinement effect of nanotubes. Moreover, the catalyst exhibits good recyclability.

## 2. Materials and Methods

All chemicals were purchased commercially and used without further purification. Magnesium nitrate (Mg(NO<sub>3</sub>)<sub>2</sub>·6H<sub>2</sub>O, Aladdin, Shanghai, China), sodium silicate (Na<sub>2</sub>SiO<sub>3</sub>·5H<sub>2</sub>O, Perimed, Beijing, China), sodium hydroxide (NaOH, Tianjin Chemical Reagent Supply and Distribution Ltd., ≥ 96.0%, Tianjin, China), ethanol absolute (CH<sub>3</sub>CH<sub>2</sub>OH, Tianjin Chemical Reagent Supply and Distribution Ltd., ≥99.7, Tianjin, China), RhCl<sub>3</sub>·nH<sub>2</sub>O (ShanxiKaida Chemical Engineering Co. Ltd. and purity ≥ 39.6%, Shanxi, China). The gases N<sub>2</sub>, CO and H<sub>2</sub> used in the experiments were all of 99.99% purity. Deionized water was used in the experiments.

### 2.1. Preparation of MgSNTs Supported Rh-nanoparticle Catalysts

The synthesis of magnesium silicate nanotubes (MgSNTs) was developed from the literature [26]. The specific steps are shown in scheme 1: 1.5 g of magnesium nitrate was dissolved in ethanol-water solution, and 10 mL sodium silicate solution (0.5 M) was added drop by drop under stirring conditions, then 2 g sodium hydroxide solid was added, stirring for 24 h. The above reaction solution was transferred to a 100 mL Teflon™ (Heze Development Zone Shengao Experimental Instrument Co., Ltd., Shandong, China) thermo reaction kettle, and the muffle furnace was heated at 200 °C for 48 h. After being centrifuged, washed and dried, the MgSNTs were obtained. MgSNTs-300 was obtained by calcining MgSNTs at 300 °C in a muffle furnace for 2 h.



**Scheme 1.** Schematic processes of preparing Rh/MgSNTs (magnesium silicate nanotubes).

The Rh/MgSNTs-300 was prepared via high temperature reduction under N<sub>2</sub> atmosphere. The synthesis of Rh/MgSNTs-300 was performed as follows: 1.0 g MgSNTs-300 was dispersed in 20 mL of aqueous RhCl<sub>3</sub> solutions (0.35 wt%, 0.5 wt%, 1.0 wt%) and vigorously agitated for 1 h. After low-energy sonication for 1h, the mixture was centrifuged and dried at 80 °C for 4 h. Then the obtained material was transferred to a tube furnace for calcination at 300 °C for 2 h under N<sub>2</sub>. The formation of Rh<sup>0</sup> in the heating procedure can be illustrated as equation (1). According to earlier data, bulk rhodium chloride decomposes to turn into Rh<sup>0</sup> at 300 °C, and the lower decomposition temperature of supported rhodium chloride may be due to its small particle size [30]. The products were marked as Rh/MgSNTs-300(a<sub>1</sub>), Rh/MgSNTs-300(a<sub>2</sub>), Rh/MgSNTs-300(a<sub>3</sub>). The Rh/MgSNTs-300(b<sub>1</sub>), Rh/MgSNTs-300(b<sub>2</sub>), Rh/MgSNTs-300(b<sub>3</sub>) was obtained by keeping rhodium content as 0.5 wt%, changing the calcination temperature to 200 °C, 400 °C and 500 °C.



## 2.2. Evaluation of Catalytic Performance of Catalysts for Hydroformylation

The catalytic activities of the catalysts for hydroformylation of vinyl acetate were measured. In a typical experiment, 0.4 g of catalyst and the required amount of substrate and solvent were placed in a 250 mL stainless steel autoclave reactor. The reactor was placed in a temperature-controlled electrical furnace and then purged with H<sub>2</sub> three times. The reactant mixture composed of CO, H<sub>2</sub> (CO/H<sub>2</sub> = 1:1) = 6.0 MPa was fed to the reactor. After this, one heated the reaction temperature to the desired pressure while stirring. When the reaction was over, the stirring was stopped.

The reactor was then cooled to room temperature and the pressure was released gradually. The product was analyzed by GC7890B-5977A MS (Agilent, Santa Clara, CA, USA) or GC (GC-2014 gas chromatograph equipped with a 30 m × 0.53 mm SE-30 capillary column and a FID, Shimadzu, Japan). Recycling uses of catalysts were carried out here simply by separating the used catalyst from the mother solution of the first reaction via centrifugation and directly used for the next run under fixed conditions.

## 2.3. Characterization

The crystal phase and structure of catalysts were detected by X-ray diffraction (XRD), Rigaku D/Max-2500, (Rigaku, Japan), which was performed with Cu–Kα radiation (λ = 1.54 Å) at 2θ from 10° to 80°. Transmission electron microscopy (TEM) images were recorded using a Tecnai G2 F20 instrument (FEI, Hillsboro, OR, USA) at an accelerating voltage of 200 kV. The X-ray photoelectron spectrometer (XPS, Kratos Axis Ultra DLD multi-technique X-ray photoelectron spectra, Kratos Analytical Ltd., Manchester, UK) was used to test the chemical states of Rh in catalysts, and all binding energies were calibrated using C1s (E<sub>b</sub> = 284.6 eV) for the reference. What needs to be noted in particular is that the XPS test was using a double anode magnesium target. The content of Rh was determined by ICP-AES (ICP-9000, USA Thermo Jarrell-Ash Corp, Franklin, MA, USA). N<sub>2</sub> adsorption/desorption isotherms were collected on an Autosorb-1-MP 1530VP (Quantachrome, Florida, FL, USA) automatic surface area and porosity analyzer. The sample was degassed at 473 K for 5 h and then analyzed at 77 K. The relative pressure (P/P<sub>0</sub>) range used for the calculation of the Brunauer–Emmett–Teller (BET) surface area was from 0.05 to 0.30.

## 3. Results and Discussion

### 3.1. GC-MS Analysis

Figure 1 shows the chromatogram after hydroformylation of vinyl acetate. GC-MS also gave peak with an m/z ratio of M. However, peaks with m/e ratios of 87 (corresponding to aldehyde loss), 43 (CH<sub>3</sub>CO)<sup>+</sup> and 29 (CHO) were observed (Figure S1), confirming that the product at 4.315 min was indeed 2-acetoxypropanal. Peak (Figure S2) with m/e ratios of 116 is the molecular ion peak of the product aldehyde. As we all know, only the stable 3-acetoxypropanal will produce molecular ion peaks. So, the other reaction product was 3-acetoxypropanal. On the other hand, the two

by-products observed were propanal (Figure S3) and ethyl acetate (Figure S4) arising from the hydrogenation of the substrate, which was similar to that observed by previous reports [28], of course, there is solvent toluene in the sample (Figure S5).

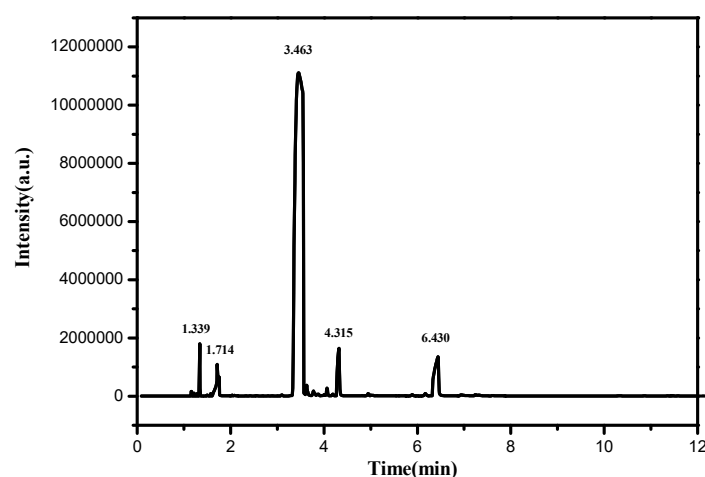


**Figure 1.** Chromatogram of hydroformylation after the reaction. Propionic (RT: 1.339 min); Ethyl acetate (RT: 1.714 min); toluene (RT: 3.463 min); 2-acetoxypropanal (RT: 4.315 min); 3-acetoxypropanal (RT: 6.430 min).

### 3.2. BET and ICP Analysis

Brunauer–Emmett–Teller (BET) analysis was used to investigate the specific surface area (SSA) of the as-prepared catalysts (Table 1). The surface area of the catalysts are calculated to be 238.2, 236.7 and 229.6  $\text{m}^2 \text{g}^{-1}$  for Rh/MgSNTs-300(a<sub>1</sub>), Rh/MgSNTs-300(a<sub>2</sub>), and Rh/MgSNTs-300(a<sub>3</sub>), respectively. The SSAs of all catalysts are significantly lower than that of pure supports (250.6  $\text{m}^2 \text{g}^{-1}$ ), which may be ascribed to those metal nanoparticles deposited on the outer and inner surface in MgSNTs like the TNTs catalysts [17,31,32]. The nanotubular structures are readily accessible, favorable to adsorption and release of reactants. The large surface areas and big size holes may combine to enhance the catalytic applications of these novel nanotube materials in the hydroformylation of olefins.

The actual content of Rh in catalysts was further studied by ICP-AES listed in Table 1. EDX detection (Figure S6) of Rh/MgSNTs-300(b<sub>1</sub>) shows clearly that there are peaks of Rh, which confirms the presence of Rh in the MgSNTs-300. The EDX shows that the content of Rh in the Rh/MgSNTs-300 is 0.6 wt%, which is higher than that in ICP result (Table 1). ICP and EDX results exhibit clearly Rh enrichment in the Rh/MgSNTs, which is favorable for utilizing Rh effectively in the hydroformylation of olefins.

**Table 1.** Brunauer–Emmett–Teller (BET) and atomic emission spectrometer (ICP-AES) data of Rh/MgSNTs-300.

Entry	Catalyst	SSA ( $\text{m}^2/\text{g}$ )	Rh Content (wt%)
1	MgSNTs-300	250.6	-
2	Rh/MgSNTs-300(a <sub>1</sub> )	238.2	0.30
3	Rh/MgSNTs-300(a <sub>2</sub> )	236.7	0.41
4	Rh/MgSNTs-300(a <sub>3</sub> )	229.6	0.72
5	Rh/MgSNTs-300(b <sub>1</sub> )	236.5	0.42
6	Rh/MgSNTs-300(b <sub>2</sub> )	218.6	0.43
7	Rh/MgSNTs-300(b <sub>3</sub> )	211.2	0.42

### 3.3. XRD Analysis

Figure 2 shows the X-ray diffraction (XRD) patterns of the as-prepared Rh/MgSNTs-300(b<sub>1</sub>), Rh/MgSNTs-300(a<sub>2</sub>), Rh/MgSNTs-300(b<sub>2</sub>) and Rh/MgSNTs-300(b<sub>3</sub>). The wide-angle XRD pattern in Figure 2 reveals that all of the samples display the diffractions of Mg<sub>3</sub>Si<sub>2</sub>O<sub>5</sub>(OH)<sub>4</sub> with lattice constants  $a = 5.33$  and  $c = 7.269$  (JCPDS no. 82-1838) [26]. Figure 2A,B show that the major peaks of Rh/MgSNTs-300(b<sub>1</sub>) and Rh/MgSNTs-300(a<sub>2</sub>) in the wide-angle XRD pattern are sharp and well-resolved, suggesting a well-defined crystalline nanostructure. Figure 3C,D show the XRD pattern of Rh/MgSNTs-300(b<sub>2</sub>) and Rh/MgSNTs-300(b<sub>3</sub>). The intensities of the peaks decrease with the increase of the calcination temperature, which indicates that the optimum calcination temperature for catalyst preparation is 300 °C. There were no peaks relevant to Rh found in Figure 2C,D, due to the relatively low content and very small size of Rh particles, which was similar to that observed by our previous reports [31].

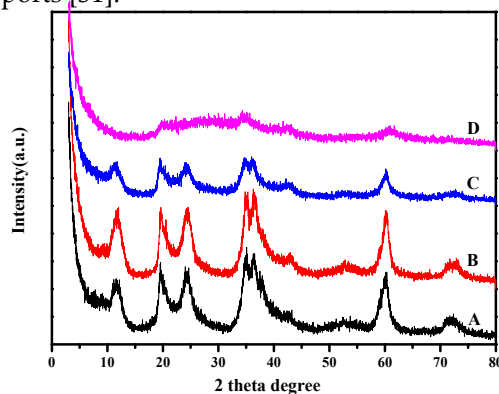


**Figure 2.** XRD patterns of (A) Rh/MgSNTs-300(b<sub>1</sub>), (B) Rh/MgSNTs-300(a<sub>2</sub>), (C) Rh/MgSNTs-300(b<sub>2</sub>), (D) Rh/MgSNTs-300(b<sub>3</sub>).

### 3.4. TEM Analysis

Figure 3 shows the TEM images of the MgSNTs-300 and Rh/MgSNTs-300. It is clear from Figure 3 that MgSNTs-300 show perfect nanotubular morphology with a length of about 200–800 nm and diameter of about 8–10 nm (Figure 3A,B). There is no obvious rupture or fracture caused by 300 °C heat treatment (Figure 3C). Rh nanoparticles are well-dispersed on the inner and outer surfaces of the nanotubes without agglomeration. Additionally, Figure 3G,H show the size distributions of particles in different catalysts. The average diameter of the Rh particles in Rh/MgSNTs-300(a<sub>1</sub>) is about 1.97 nm (Figure 3G), which is obviously smaller than that in Rh/MgSNTs-300(b<sub>2</sub>) (2.75 nm, Figure 3H), and the size distributions of particles are in a relatively narrow range. The increase of Rh nanoparticles' size in Rh/MgSNTs-300(b<sub>2</sub>) is due to the increase of calcination temperature. There were no obvious Rh nanoparticles in Rh/MgSNTs-300(a<sub>2</sub>), which was calcined at 200 °C (Figure 3B). The possible reason is that 200 °C is not enough for RhCl<sub>3</sub> to decompose into metallic Rh nanoparticles. There are obviously ruptures and fractures caused by 400 °C and 500 °C calcination (Figure 3E, F).

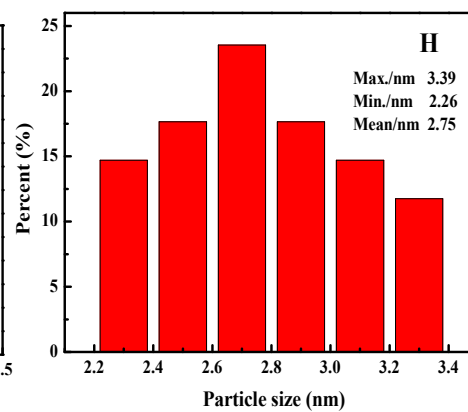
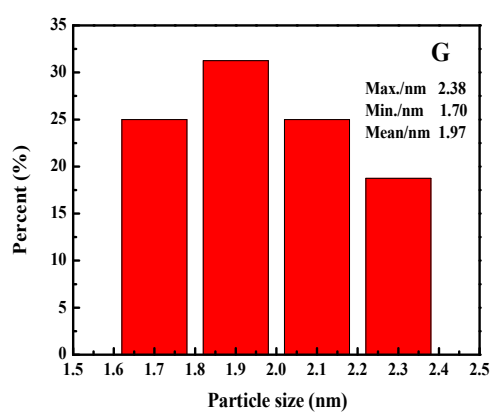
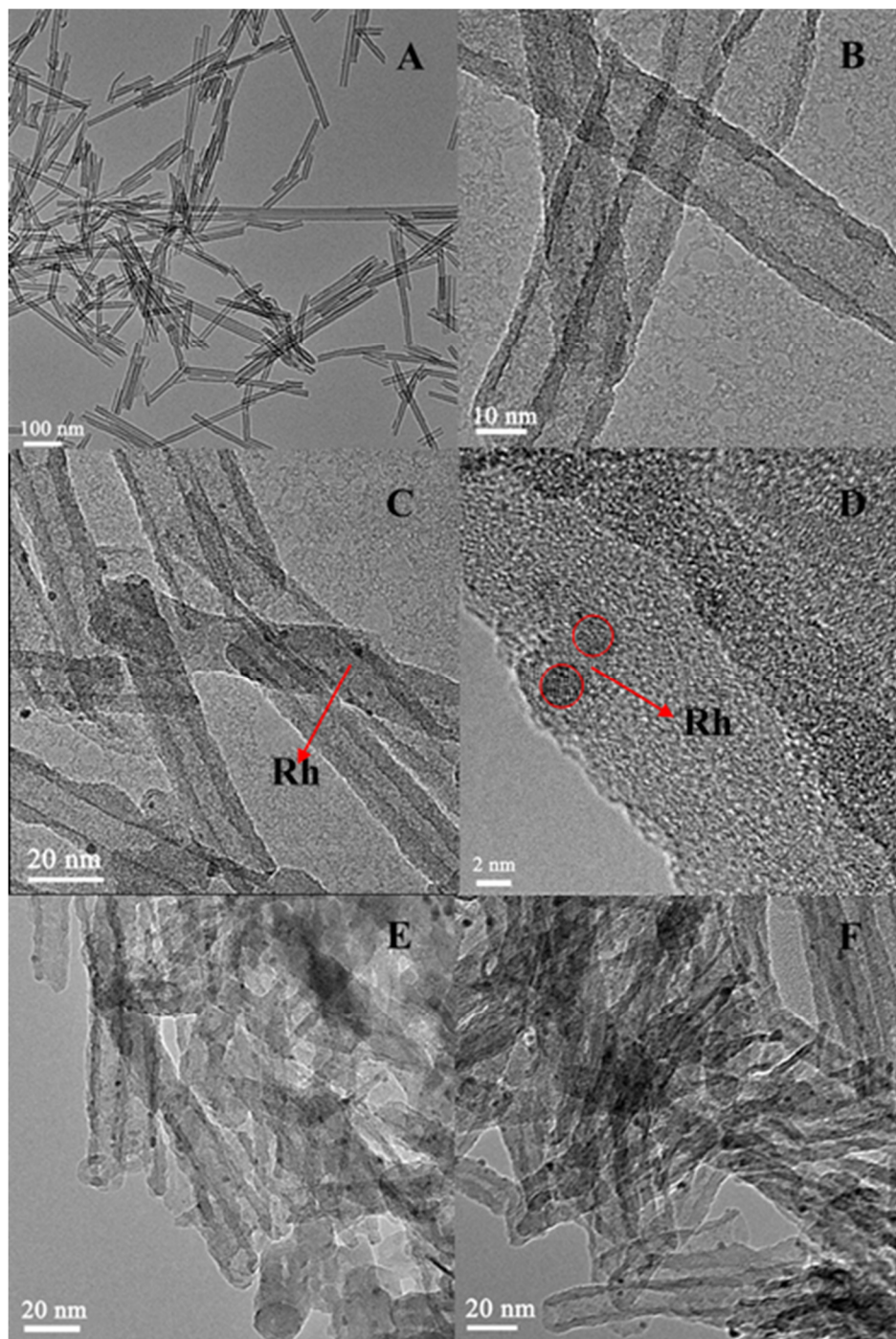


**Figure 3.** Transmission electron microscopy (TEM) images of (A) MgSNTs-300; (B) Rh/MgSNTs-300(b<sub>1</sub>); (C) Rh/MgSNTs-300(a<sub>1</sub>); (D) High resolution of Rh/MgSNTs-300(a<sub>1</sub>); (E) Rh/MgSNTs-300(b<sub>2</sub>); (F) Rh/MgSNTs-300(b<sub>3</sub>). Size distributions of particles in (G) Rh/MgSNTs-300(a<sub>1</sub>); (H) Rh/MgSNTs-300(b<sub>2</sub>).

### 3.5. XPS Analysis

XPS was performed to evaluate the chemical state of the catalysts. As shown in Figure 4, Rh 3d<sub>5/2</sub> and Rh 3d<sub>3/2</sub> show that the group peaks not only centered at 307.1 and 311.8 eV, but also at 309.1 and 314.0 eV. These indicate that Rh exists in two forms of Rh<sup>0</sup> (307.1 and 311.8 eV) [33] and oxidation state (309.1 and 314.0 eV). The higher binding energy state should have relevance to the partially oxidized Rh<sup>2+</sup> ions [25]. It is well-known that Rh<sup>0</sup> is the active site for the hydroformylation of olefins [31]. The percentage of Rh<sup>0</sup> in rhodium is calculated based on the area of the fitted Gauss peaks, with the proportions of Rh<sup>0</sup> in Rh/MgSNTs-300(a<sub>1</sub>) at 89.79%. Thus, the XPS data showed that RhCl<sub>3</sub> can be decomposed into Rh<sup>0</sup> at 300 °C heat treatment.

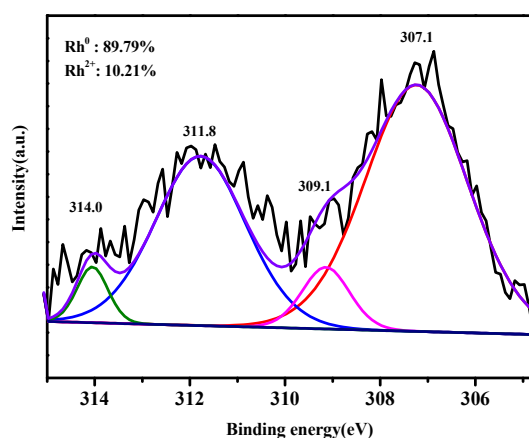
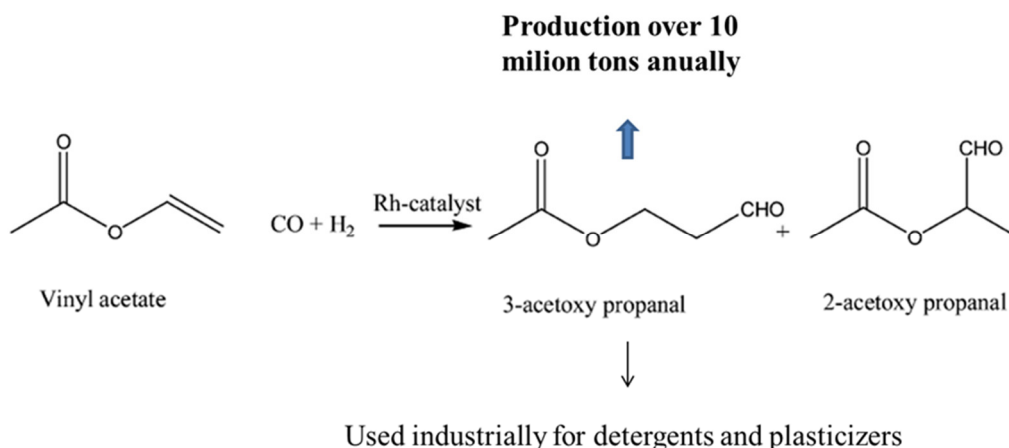


**Figure 4.** XPS spectrum of Rh/MgSNTs-300(a<sub>1</sub>).

### 3.6. Catalytic Activity Evaluation

Scheme 2 shows the possible aldehydes formed in the hydroformylation reaction of vinyl acetate.



**Scheme 2.** Hydroformylation of vinyl acetate.

In the real hydroformylation reaction of vinyl acetate, the main reaction products were 2-acetoxypropanal (major) and 3-acetoxypropanal with acetic acid, propanal, and ethyl acetate as

side products [28]. The GC and MS fragments of products formed in the hydroformylation of vinyl acetate are shown in the supporting information (Figure S1–S5).

The influence of the different Rh contents on catalytic performances was investigated. Shown in Table 2 is that of the Rh/MgSNTs-300 catalysts with various Rh contents. It can be seen that increasing Rh content can remarkably enhance the conversion of vinyl acetate and TOF.

But the selectivity of linear aldehyde (3-acetoxy propanal) decreases obviously with the increase of Rh content from 0.5 wt% to 1.0 wt%. This might be due to little Rh content in the inner surface of the nanotubes. Most Rh nanoparticles loaded in the outer surface of the nanotubes with the theoretical Rh content, increased from 0.5 wt% to 1.0 wt%. This is because Rh in the inner surface of the nanotubes is beneficial to the formation of linear aldehydes, because the spatial confinement effect of the tube hinders the formation of branched aldehyde. The optimum Rh loading should be about 0.5 wt% and the proportion of the linear aldehyde (3-acetoxy propanal) can reach 9%.

**Table 2.** Effect of Rh content on the hydroformylation over Rh/MgSNTs<sup>a</sup>.

Catalyst	Theoretical load ICP	Rh content (wt%)	Conversion (%)	TOF <sup>b</sup> (h <sup>-1</sup> )	Aldehyde (%)	b:l <sup>c</sup>
Rh/MgSNTs-300(a <sub>1</sub> )	0.35	0.16	74	82	69	96:4
Rh/MgSNTs-300(a <sub>2</sub> )	0.5	0.31	97	161	74	91:9
Rh/MgSNTs-300(a <sub>3</sub> )	1.0	0.53	99	181	75	95:5

<sup>a</sup> Reaction conditions: vinyl acetate = 5 mL, catalyst = 0.40 g, temp. = 110 °C, syngas pressure = 6.0 MPa, CO:H<sub>2</sub> = 1, solvent (toluene) = 65 mL, and reaction time = 8 h. <sup>b</sup> TOF is calculated by the formula  $TOF = \frac{n(\text{aldehydes})}{n(\text{Rh}) \times h}$ ,  $n(\text{aldehydes})$  is the total moles of aldehydes,  $n(\text{Rh})$  is the total moles of Rh in the catalyst. <sup>c</sup> b:l is branched aldehyde (2-acetoxy propanal): linear aldehyde (3-acetoxy propanal).

Table 3 shows the effect of reaction temperature on the Rh/MgSNTs-300 catalyzed hydroformylation reaction of vinyl acetate. Table 3 shows that the conversion of vinyl acetate and the selectivity of linear aldehyde, both increased along with the increase in reaction temperature from 60 °C to 110 °C. When the reaction temperature increased from 110 °C to 120 °C, the conversion of vinyl acetate kept on rising. However, the total amount of aldehydes, and the selectivity of linear aldehyde were all decreased, indicating that increasing the temperature was more favorable for the hydrogenation of vinyl acetate. Thus, it can be concluded that the suitable reaction temperature should be 110 °C.

**Table 3.** Effect of reaction temperatures on the Rh/MgSNTs-300 catalyzed hydroformylation reaction of vinyl acetate<sup>a</sup>.

Catalyst	Temperature (°C)	Conversion (%)	By products (%)		TOF <sup>b</sup> (h <sup>-1</sup> )	Aldehyde (%)	b:l <sup>c</sup>
			propanal	ethyl acetate			
Rh/MgSNTs-300(a <sub>2</sub> )	60	22	22	13	29	65	99:1
Rh/MgSNTs-300(a <sub>2</sub> )	80	43	23	15	68	62	98:2
Rh/MgSNTs-300(a <sub>2</sub> )	110	90	24	11	161	68	91:9
Rh/MgSNTs-300(a <sub>2</sub> )	120	92	25	11	179	64	95:5

<sup>a</sup> Reaction conditions: vinyl acetate = 5 mL, Catalyst = 0.40g, syngas pressure = 6.0 MPa, CO:H<sub>2</sub> = 1, solvent (toluene) = 65 mL, and reaction time = 8 h. <sup>b</sup> TOF is calculated by the formula  $TOF = \frac{n(\text{aldehydes})}{n(\text{Rh}) \times h}$ ,  $n(\text{aldehydes})$  is the total moles of aldehydes,  $n(\text{Rh})$  is the total moles of Rh in catalyst.

<sup>c</sup> b:l is branched aldehyde (2-acetoxy propanal): linear aldehyde (3-acetoxy propanal).

Shown in Table 4 are the catalytic performances of Rh/MgSNTs catalysts with various calcination temperatures. It can be seen that calcination temperature can obviously affect catalytic activity. The conversion of vinyl acetate, the selectivity for aldehyde and TOF were all increased with the increase of calcination temperature from 200 to 400 °C. But the difference between Rh/MgSNTs-300(a<sub>2</sub>) and Rh/MgSNTs-300(b<sub>2</sub>) was not obvious. However, the catalytic activity

decreased significantly with the increase of calcination temperature from 400 to 500 °C. The possible explanation is that 200 °C was not enough to get Rh<sup>0</sup>, since most of Rh was in oxidation state (Confirmed by XPS). On the other hand, excessive temperature caused fragmentation of some nanotubes (Confirmed by TEM). Moreover, the selectivity of linear aldehydes was reduced because the tubular structure was destroyed due to high temperature calcination, and there was no spatial confinement effect. Thus, the optimum calcination temperature should be about 300 °C.

**Table 4.** Effect of calcination temperature of catalyst on hydroformylation of vinyl acetate<sup>a</sup>.

Catalyst	Calcination temperature (°C)	Conversion (%)	TOF <sup>b</sup> (h <sup>-1</sup> )	Aldehyde (%)	b:l <sup>c</sup>
Rh/MgSNTs-300(b <sub>1</sub> )	200	68	101	45	99:1
Rh/MgSNTs-300(a <sub>2</sub> )	300	97	161	68	91:9
Rh/MgSNTs-300(b <sub>2</sub> )	400	91	165	69	92:8
Rh/MgSNTs-300(b <sub>3</sub> )	500	75	132	56	98:2

<sup>a</sup> Reaction conditions: vinyl acetate = 5 mL, catalyst = 0.40 g, temp.= 110 °C, syngas pressure = 6.0 MPa, CO:H<sub>2</sub> = 1, solvent (toluene) = 65 mL, and reaction time = 8 h. <sup>b</sup> TOF is calculated by the formula  $TOF = \frac{n(\text{aldehydes})}{n(\text{Rh}) \times h}$ ,  $n(\text{aldehydes})$  is the total moles of aldehydes,  $n(\text{Rh})$  is the total moles of Rh in catalyst.

<sup>c</sup> b:l is branched aldehyde (2-acetoxy propanal): linear aldehyde (3-acetoxy propanal).

The stability of catalysts is important for the hydroformylation of olefins for practical application. Nowadays, Karakhanov [34] and coworkers reported that Rh-containing catalysts immobilized on a hybrid organic–inorganic surface for hydroformylation of 1-octene. The activity of the catalyst decreased significantly after four cycles.

To investigate the stability of our catalysts, Rh/MgSNTs-300(a<sub>2</sub>) was selected for recycle catalytic experiments. The experimental results are listed in Table 5. As can be seen from Table 5, Rh/MgSNTs-300(a<sub>2</sub>) remained highly active and the yield of aldehyde maintained at around 54% in the fourth recycle. The rhodium content in the solution after the reaction was tested by ICP (listed in Table 6). The experimental results show that the catalyst had good stability. This may be because the calcination can significantly enhance the interaction between MgSNTs-300 and Rh.

**Table 5.** Studies of catalyst stability<sup>a</sup>.

Catalyst	Cycle Times	Conversion (%)	By products (%)		Aldehyde (%)	b:l <sup>b</sup>
			propanal	ethyl acetate		
Rh/MgSNTs-300(a <sub>2</sub> )	1	97	19	13	68	91:9
Rh/MgSNTs-300(a <sub>2</sub> )	2	82	19	15	66	92:8
Rh/MgSNTs-300(a <sub>2</sub> )	3	74	23	19	58	95:5
Rh/MgSNTs-300(a <sub>2</sub> )	4	58	24	22	54	97:3

<sup>a</sup> Reaction conditions: vinyl acetate = 5 mL, Rh/MgSNTs-300(a<sub>2</sub>) = 0.40 g, temp.= 110°C, syngas pressure = 6.0 MPa, CO:H<sub>2</sub> = 1, solvent (toluene) = 65 mL, and reaction time = 8 h. <sup>b</sup> b:l is branched aldehyde (2-acetoxy propanal): linear aldehyde (3-acetoxy propanal).

**Table 6.** Rhodium content in the solution after the reaction.

Catalyst	Cycle Times	Rh (PPM)
Rh/MgSNTs-300	1	20.3
Rh/MgSNTs-300	2	16.4
Rh/MgSNTs-300	3	15.7
Rh/MgSNTs-300	4	9.7

#### 4. Conclusions

In this article, a simple and efficient heating preparation route was used to prepare Rh/MgSNTs catalyst. Rh particles were uniformly deposited on the outer and inner surface of MgSNTs. MgSNTs

plays an important role in fastening the Rh nanoparticles. The as-prepared Rh/MgSNTs(a<sub>2</sub>) catalyst shows regioselectivity (9%) to linear aldehyde (3-acetoxy propanal). Although the selectivity has been greatly improved compared with some recent literatures, it still has no industrial value. We observed a modest decrease of activity with the recycling of the catalyst, the selectivity decreasing quite a bit from 97% to 58%, and this should be due to the loss of Rh during the reaction (Rh leaching was observed in Table 6). Studies to obtain higher 3-acetoxy propanal selectivity and more stable catalysts are underway in our laboratory.

**Supplementary Materials:** Figure S1: GC-MS chromatogram of hydroformylation: propionic aldehyde (RT: 1.399 min). Figure S2: GC-MS chromatogram of hydroformylation: ethyl acetate (RT: 1.714 min). Figure S3: GC-MS chromatogram of hydroformylation: toluene (RT: 3.463 min). Figure S4 GC-MS chromatogram of hydroformylation: 2-acetoxypropanal (RT: 4.315 min). Figure S5 GC-MS chromatogram of hydroformylation: 3-acetoxypropanal (RT: 6.430 min). Figure S6 EDX detection of Rh/MgSNTs-300(b<sub>1</sub>).

**Author Contributions:** P.S. performed the experiments and wrote the original draft; Y.C., X.L., H.C., H.L. done the work of data processing; B.Z., S.Z. and W.H. conceived the concept. All the authors contributed to the writing of the manuscript.

**Funding:** This work is supported by the National Natural Science Foundation of China (21373120 and 21071086) and 111 Project (B12015).

**Acknowledgments:** This research has no external acknowledgments.

**Conflicts of Interest:** The authors declare no conflict of interest.

## References

1. Su, J.; Xie, C.L.; Chen, C.; Yu, Y.; Kennedy, G.; Somorjai, G.A.; Yang, P.D. Insights into the Mechanism of Tandem Alkene Hydroformylation over a Nanostructured Catalyst with Multiple Interfaces. *J. Am. Chem. Soc.* **2016**, *138*, 11568–11574. DOI: 10.1021/jacs.6b03915
2. You, C.; Li, X.X.; Yang, Y.H.; Yang, Y.S.; Tan, X.F.; Li, S.L.; Wei, B.; Lv, H.; Chung, L.W.; Zhang, X.M. Silicon-oriented regio- and enantioselective rhodium-catalyzed hydroformylation. *Nat. Commun.* **2018**, *9*, 2045. DOI: 10.1038/s41467-018-04277-7
3. Wu, Q.H.; Zhou, F.D.; Shu, X.; Jian, J.; Xu, B.; Zheng, X.L.; Yuan, M.L.; Fu, H.Y.; Li, R.X.; Chen, H. Synthesis and application of PNP pincer ligands in rhodium-catalyzed hydroformylation of cycloolefins. *RSC Adv.* **2016**, *6*, 107305–107309. DOI: 10.1039/C6RA24144A
4. Nelsen, E.R.; Brezny, A.C.; Landis, C.R. Interception and Characterization of Catalyst Species in Rhodium Bis (diazaphospholane)-Catalyzed Hydroformylation of Octene, Vinyl Acetate, Allyl Cyanide, and 1-Phenyl-1,3-butadiene. *J. Am. Chem. Soc.* **2015**, *137* (44), 14208–14219. DOI: 10.1021/jacs.5b09858
5. Chen, C.Y.; Dong, X.Q.; Zhang, X.M. Chiral Ligands for Rhodium-Catalyzed Asymmetric Hydroformylation: A Personal Account. *Chem. Rec.* **2016**, *16*, 2674–2686.
6. Schmitz, C.; Holthausen, K.; Leitner, W.; Francio, G. Highly Regio- and Enantioselective Hydroformylation of Vinyl Esters Using Bidentate Phosphine, P-Chiral Phosphorodiamidite Ligands. *ACS Catal.* **2016**, *6* (3), 1584–1589. DOI: 10.1021/acscatal.5b02846
7. Ma, Y.B.; Qing, S.J.; Yin, D.; Mamat, X.; Zhang, J.; Gao, Z.X.; Wang, T.F.; Eli, W. Rh-based catalysts supported on MCM-41-type mesoporous silica for dicyclopentadiene hydroformylation. *Catal. Today* **2015**, *258*, 64–69. <https://doi.org/10.1016/j.cattod.2015.04.007>
8. Ma, Y.B.; Fu, J.; Gao, Z.X.; Zhang, L.B.; Li, C.Y.; Wang, T.F.; Dicyclopentadiene Hydroformylation to Value-Added Fine Chemicals over Magnetically Separable Fe<sub>3</sub>O<sub>4</sub>-Supported Co-Rh Bimetallic Catalysts: Effects of Cobalt Loading. *Catalysts* **2017**, *7* (4), 103. DOI:10.3390/catal7040103
9. Schmidt, S.; Deglmann, P.; Hofmann, P. Density Functional Investigations of the Rh-Catalyzed Hydroformylation of 1,3-Butadiene with Bisphosphite Ligands. *ACS Catal.* **2014**, *4* (10), 3593–3604. DOI: 10.1021/cs500718v
10. Wu, L.Q.; Liu, Q.; Spannenberg, A.; Jackstell, R.; Beller, M.; Highly regioselective osmium-catalyzed hydroformylation. *Chem. Commun.* **2015**, *51*, 3080–3082. DOI: 10.1039/C4CC05626D
11. Piras, I.; Jennerjahn, R.; Jackstell, R.; Spannenberg, A.; Franke, R.; Beller, M.; A General and Efficient Iridium-Catalyzed Hydroformylation of Olefins. *Angew. Chem. Int. Ed.* **2011**, *123*, 280–284. <https://doi.org/10.1002/anie.201001972>

12. Lang, R.; Li, T.B.; Matsumura, D.J.; Miao, S.; Ren, Y.J.; Cui, Y.T.; Tan, Y.; Qiao, B.T.; Li, L.; Wang, A.Q.; Wang, X.D.; Zhang, T. Hydroformylation of Olefins by a Rhodium Single-Atom Catalyst with Activity Comparable to  $\text{RhCl}(\text{PPh}_3)_3$ . *Angew. Chem. Int. Ed.* **2016**, *55*, 16054–16058. <https://doi.org/10.1002/ange.201610872>
13. Bocokić, V.; Kalkan, A.; Lutz, M.; Spek, A.L.; Gryko, D.T.; Reek, J.N.H. Capsule-controlled selectivity of a rhodium hydroformylation catalyst. *Nat. Commun.* **2013**, *4*, 2670. <http://dx.doi.org/10.1038/ncomms3670>
14. Benetskiy, E.; Lühr, S.; Vilches-Herrera, M.; Selent, D.; Jiao, H.J.; Domke, L.; Dyballa, K.; Franke, R.; Börner, A. Rhodium-Catalyzed Nonisomerizing Hydroformylation of Methyl Oleate Applying Lactame-Based Phosphoramidite Ligands. *ACS Catal.* **2014**, *4* (7), 2130–2136. DOI: 10.1021/cs500274n
15. Cardozo, A.F.; Julcour, C.; Barthe, L.; Blanco, J.F.; Chen, S.; Gayet, F.; Manoury, E.; Zhang, X.W.; Lansalot, M.; Charleux, B.; D'Agosto, F.; Poli, R.; Delmas, H. Aqueous phase homogeneous catalysis using core-shell nanoreactors: Application to rhodium-catalyzed hydroformylation of 1-octene. *J. Catal.* **2015**, *324*, 1–8. <http://dx.doi.org/10.1016/j.jcat.2015.01.009>
16. Dahl, J.A.; Maddux, B.L.S.; Hutchison, J.E. Toward Greener Nanosynthesis. *Chem. Rev.* **2007**, *107*, 2228–2269. DOI: 10.1021/cr050943k
17. Chuai, H.Y.; Liu, X.T.; Chen, Y.; Zhu, B.L.; Zhang, S.M.; Huang, W.P. Hydroformylation of vinyl acetate and cyclohexene over  $\text{TiO}_2$  nanotube supported Rh and Ru nanoparticle catalysts. *RSC Adv.* **2018**, *8*, 12053–12059. DOI: 10.1039/C8RA01399C
18. Chen, Y.; Su, P.H.; Liu, T.; Liu, H.C.; Zhu, B.L.; Zhang, S.M.; Huang, W.P. Titanate nanotube-supported Au-Rh bimetallic catalysts: characterization and their catalytic performances in hydroformylation of vinyl acetate. *Catalysts* **2018**, *8*, 420–433.
19. Kwon, Y.; Kim, T.Y.; Kwon, G.; Yi, J.; Lee, H. Selective Activation of Methane on Single-Atom Catalyst of Rhodium Dispersed on Zirconia for Direct Conversion. *J. Am. Chem. Soc.* **2017**, *139*, 17694–17699. DOI: 10.1021/jacs.7b11010
20. Chen, F.; Jiang, X.Z.; Zhang, L.L.; Lang, R.; Qiao, B.T. Single-atom catalysis: Bridging the homo- and heterogeneous catalysis Chinese. *J. Catal.* **2018**, *39*, 893–898. [https://doi.org/10.1016/S1872-2067\(18\)63047-5](https://doi.org/10.1016/S1872-2067(18)63047-5).
21. Guan, E.; Gates, B.C.; Stable Rhodium Pair Sites on MgO: Influence of Ligands and Rhodium Nuclearity on Catalysis of Ethylene Hydrogenation and H-D Exchange in the Reaction of  $\text{H}_2$  with  $\text{D}_2$ . *ACS Catal.* **2018**, *8*, 482–487. DOI: 10.1021/acscatal.7b03549
22. Vunain, E.; Ncube, P.; Jalama, K.; Meijboom, R. Confinement effect of rhodium(I) complex species on mesoporous MCM-41 and SBA-15: effect of pore size on the hydroformylation of 1-octene. *J. Porous. Mater.* **2018**, *25*, 303–320. DOI 10.1007/s10934-017-0443-9
23. Ahmed, M.; Sakthivel, A. Covalent grafting of cobalt carbonyl cluster on functionalized mesoporous SBA-15 molecular sieve and its applications towards hydroformylation of 1-octene. *J. Mol. Catal. A-Chem.* **2016**, *424*, 85–90. <https://doi.org/10.1016/j.molcata.2016.08.016>
24. Wang, Y.Q.; Yan, L.; Li, C.Y.; Jiang, M.; Wang, W.L.; Ding, Y.J. Highly efficient porous organic copolymer supported Rh catalysts for heterogeneous hydroformylation of butenes. *Appl. Catal. A-Gen* **2018**, *551*, 98–105. <https://doi.org/10.1016/j.apcata.2017.12.013>
25. Shi, Y.K.; Hu, X.J.; Zhu, B.L.; Wang, S.R.; Zhang, S.M.; Huang, W.P. Synthesis and characterization of  $\text{TiO}_2$  nanotube supported Rh-nanoparticle catalysts for regioselective hydroformylation of vinyl acetate. *RSC Adv.* **2014**, *4*, 62215–62222. DOI: 10.1039/C4RA11156G
26. Du, X.J.; Fu, N.H.; Zhang, S.L.; Chen, C.; Wang, D.S.; Li, Y.D. Au/CuSiO<sub>3</sub> nanotubes: High-performance robust catalysts for selective oxidation of ethanol to acetaldehyde. *Nano Res.* **2016**, *9* (9): 2681–2686. DOI: 10.1007/s12274-016-1155-1
27. Su, P.H.; Zhen, L.A.; Chen, Y.; Liu, X.T.; Zhu, B.L.; Zhang, S.M.; Huang, W.P. Catalytic performance for hydroformylation of cyclohexene of MgSNTs-supported amorphous Co-B catalyst. *Chinese J. Inorg. Chem.* **2018**, *34*, 2197–2204. DOI:10.11862/CJIC.2018.275
28. Khan, S.R.; Bhanage, B.M. Regioselective hydroformylation of vinyl esters catalyzed by  $\text{Rh}(\text{acac})(\text{CO})_2$  with simple and efficient diphosphinite ligands. *Catal. Commun.* **2014**, *46*, 109–112. <https://doi.org/10.1016/j.catcom.2013.12.002>
29. Nelsen, E.R.; Brezny, A.C.; Landis, C.R. Interception and Characterization of Catalyst Species in Rhodium Bis(diazaphospholane)-Catalyzed Hydroformylation of Octene, Vinyl Acetate, Allyl Cyanide, and 1-Phenyl-1,3-butadiene. *J. Am. Chem. Soc.* **2015**, *137*, 14208–14219. DOI: 10.1021/jacs.5b09858

30. Simagina, V.I.; Netskina, O.V.; Komova, O.V.; Odegova, G.V.; Kochubei, D.I.; Ishchenko, A.V. Activity of Rh/TiO<sub>2</sub> Catalysts in NaBH<sub>4</sub> Hydrolysis: The Effect of the Interaction between RhCl<sub>3</sub> and the Anatase Surface during Heat Treatment. *Kinet. Catal.* **2008**, *49*, 568–573. <https://doi.org/10.1134/S0023158408040174>
31. Su, P.H.; Liu, X.T.; Chen, Y.; Liu, H.C.; Zhu, B.L.; Zhang, S.M.; Huang, W.P. Synthesis and characterization of Rh/B-TNTs as a recyclable catalyst for hydroformylation of olefin containing -CN functional group. *Nanomaterials* **2018**, *8*, 755. doi:10.3390/nano8100755
32. Shi, Y.K.; Hu, X.J.; Chen, L.; Lu, Y.; Zhu, B.L.; Zhang, S.M.; Huang, W.P. Boron modified TiO<sub>2</sub> nanotubes supported Rh-nanoparticle catalysts for highly efficient hydroformylation of styrene. *New J. Chem.* **2017**, *41*, 6120. DOI: 10.1039/c7nj01050h
33. Simagina, V.I.; Storozhenko, P.A.; Netskina, O.V.; Komova, O.V.; Odegova, G.V.; Larichev, Y.V.; Ishchenko, A.V.; Ozerova, A.M. Development of catalysts for hydrogen generation from hydride compounds. *Catal. Today* **2008**, *138*, 253–259. doi:10.1016/j.cattod.2008.05.022
34. Gorbunov, D.; Safronova, D.; Kardasheva, Y.; Maximov, A.; Rosenberg E.; Karakhanov E. New heterogeneous Rh-Containing catalysts immobilized on a hybrid organic–inorganic surface for hydroformylation of unsaturated compounds. *ACS Appl. Mater. Interfaces* **2018**, *10*, 26566–26575. DOI:10.1021/acsami.8b02797



© 2019 by the authors. Licensee MDPI, Basel, Switzerland. This article is an open access article distributed under the terms and conditions of the Creative Commons Attribution (CC BY) license (<http://creativecommons.org/licenses/by/4.0/>).